



THE UNIVERSITY *of* EDINBURGH

Edinburgh Research Explorer

Inhibition effect of different interstitial materials on thermal runaway propagation in the cylindrical lithium-ion battery module

Citation for published version:

Yuan, C, Wang, Q, Wang, Y & Zhao, Y 2019, 'Inhibition effect of different interstitial materials on thermal runaway propagation in the cylindrical lithium-ion battery module', *Applied Thermal Engineering*, vol. 153, pp. 39-50. <https://doi.org/10.1016/j.applthermaleng.2019.02.127>

Digital Object Identifier (DOI):

[10.1016/j.applthermaleng.2019.02.127](https://doi.org/10.1016/j.applthermaleng.2019.02.127)

Link:

[Link to publication record in Edinburgh Research Explorer](#)

Document Version:

Peer reviewed version

Published In:

Applied Thermal Engineering

General rights

Copyright for the publications made accessible via the Edinburgh Research Explorer is retained by the author(s) and / or other copyright owners and it is a condition of accessing these publications that users recognise and abide by the legal requirements associated with these rights.

Take down policy

The University of Edinburgh has made every reasonable effort to ensure that Edinburgh Research Explorer content complies with UK legislation. If you believe that the public display of this file breaches copyright please contact openaccess@ed.ac.uk providing details, and we will remove access to the work immediately and investigate your claim.



1 **Inhibition effect of different interstitial materials on thermal runaway**
2 **propagation in the cylindrical lithium-ion battery module**

3

4 Chengchao Yuan^{a,b}, Qingsong Wang^c, Yu Wang^d, Yang Zhao^{a,b*}

5 ^a Department of Precision Machinery and Precision Instrumentation, University of Science and
6 Technology of China, Hefei, Anhui 230027, PR China

7 ^b CAS Key Laboratory of Mechanical Behavior and Design of Materials, University of Science and
8 Technology of China, Hefei, Anhui 230027, PR China

9 ^c State Key Laboratory of Fire Science, University of Science and Technology of China, Hefei 230026,
10 PR China

11 ^d School of Engineering, BRE Centre for Fire Safety Engineering, University of Edinburgh,
12 Edinburgh EH9 3JL, United Kingdom

13

14

Nomenclature

A	surface area [m ²]
C_{can}	average mass specific heat of the can and cell material residual [J kg ⁻¹ K ⁻¹]
C_{cell}	average mass specific heat of the vented cell materials [J kg ⁻¹ K ⁻¹]
C_{total}	average mass specific heat of single cell [J kg ⁻¹ K ⁻¹]
h_{conv}	convective heat transfer coefficient [W m ⁻² K ⁻¹]
k	effective thermal conductivity [W m ⁻¹ K ⁻¹]
m_{cell}	mass of an 18650 cell's components [kg]
m_{can}	mass of an 18650 cell's stainless-steel casing [kg]
m_{total}	mass of an 18650 cell [kg]
\dot{Q}_{conv}	convective heat transfer at the cell boundaries [W m ⁻²]
\dot{Q}_{rad}	radiative heat transfer at the cell boundaries [W m ⁻²]
\dot{Q}_r	chemical reaction heat generation rate [W]
\dot{Q}_f	solid electrolyte interface (SEI) decomposition heat generation rate [W]

\dot{Q}_n	Negative-Solvent reaction heat generation rate [W]
\dot{Q}_p	Positive-Solvent reaction heat generation rate [W]
\dot{Q}_e	electrolyte decomposition heat generation rate [W]
t	time [s]
T	temperature [K]
T_0	initial exothermic temperature [K]
dT/dt	the derivative of the temperature [K s ⁻¹]
<i>Greek symbols</i>	
ε	Emissivity of the battery surface
σ	Stefan-Boltzmann constant, 5.67e-8 [W m ⁻² K ⁻⁴]
TR_T	TR triggering temperature

15 **HIGHLIGHTS**

- 16 Inhibition effect of interstitial materials on TR in battery modules is studied.
 17 CFD model is used to analyze battery temperature under different conditions.
 18 The simulation is experimentally compared and verified by basic safety units.
 19 Composite graphite sheet and Al extrusion can effectively control the thermal path.

20

21 **ABSTRACT**

22 With the growing demand for high specific energy density of lithium-ion battery
 23 pack in electric vehicle to relieve range anxiety, thermal stability in abused conditions
 24 is becoming increasingly important in battery pack safety design. Most of the fire
 25 accidents are resulted from the thermal runaway (TR) of a single cell and then propagate
 26 to the battery modules and entire pack. This study focuses on the safety enhancement
 27 methods for battery module, which is filled with different interstitial materials. The
 28 basic safety unit is composed of 11 commercial 18650 cylindrical cells, which is
 29 isolated from the electric vehicle pack as the test module. The test modules were
 30 intentionally triggered into TR by heating wire to evaluate the TR propagation

31 resistance. A model based on finite volume method was established to simulate the TR
32 propagation. The results of both simulation and experiments show that the protection
33 of neighboring cells from different interstitial materials varies significantly. Graphite
34 composite sheet and Al extrusion as interstitial materials could effectively suppress TR
35 propagation. The results also indicate that for safety design of battery pack, thermal
36 path should be effectively controlled, and particularly the combustion of expelled
37 electrolyte must be directed away from adjacent cells.

38

39 **Key words:** Electric vehicle; Lithium-ion battery safety; Thermal runaway; Interstitial
40 material; Thermal runaway propagation

41

42 **1. Introduction**

43 Lithium-ion (Li-ion) batteries, as the state-of-the-art energy storage units, have
44 been mainly applied in the fields of Energy Storage System (ESS) [1], such as Electric
45 Vehicle (EV) [2], auxiliary power unit (APU), smart grids, etc. The industry of EV has
46 boomed worldwide since 2009 due to the concerns of dependence on oil-based fuels
47 consumption and the pressure of carbon emissions. Battery electric vehicles access the
48 mass market rapidly with their advantages of zero emission and also the generous
49 subsidies from governments. Rechargeable li-ion batteries have been widely used in
50 consumer electronic devices, such as cell phones and computers [3-6]. Due to its high
51 gravimetric and volumetric energy densities [7], Li-ion battery is currently the best
52 power source candidate for BEV compared to NiMH or lead-acid battery. However,
53 higher energy density may cause greater thermal hazard if this energy is released
54 abruptly because of contamination, manufacturing defect, mechanical insult,
55 overcharging or internal short circuit caused by overheating [8-10], etc. The rapid
56 discharge of electrical energy inside the cell will raise its temperature and causes series
57 reactions, including 1) reaction between cathode and electrolyte; 2) thermal
58 decomposition of electrolyte; 3) reaction between electrolyte and anode; 4) thermal

59 decomposition of anode; 5) thermal decomposition of cathode [11-13]. This auto-
 60 acceleratory exothermic process is called thermal runaway (TR), which generates
 61 combustible gases, and results in expulsions of the cell components [14-16]. Generally,
 62 there are three ways to improve the safety performance of lithium-ion battery to prevent
 63 TR: 1) enhance thermal stability of the electrode materials; 2) improve the electrolyte
 64 of lithium-ion battery to avoid burning; 3) propose new design and management of
 65 lithium-ion battery through some external methods, such as safety design and insulation
 66 of cells, safety valves and the process improvement [17-19].

67 The safety issues of Li-ion batteries have drawn tremendous attention and become
 68 an urgent problem to be solved in the development of Li-ion batteries. Some typical
 69 battery pack safety accidents are shown in Table 1. However, the risk of thermal
 70 runaway becomes even more severe in large scale battery pack since failure of a single
 71 cell could trigger a TR propagation in the whole pack, which may cause catastrophic
 72 damages.

73

74 **Table 1**

75 Typical accidents related to Li-ion batteries

Date/Place	Brand	Power type	Cause
May 2011/USA	Chevrolet Volt	BEV	Caught fire after crash test
2012/Texas	Fisker Karma	HEV	Unknown
Jan 7 2013/Boston's Logan International Airport	Boeing 787 Dreamliner	APU	Internal short circuit
Jan 1 2016/ Norway Gjerstad	Tesla MODEL S	BEV	Distribution box short circuit
Apr 9 2016/Shanghai	BYD	HEV	Foreign body in exhaust pipe
May 14 2016/Zhuhai	Yinlong	BEV	Battery short circuit
June 23 2016/Beijing	JAC iEV5	BEV	Unknown

76

77 For a battery pack that is in working status, there are several factors that may lead
 78 to thermal runaway, such as mechanical abuse (puncture, crush), electrical abuse
 79 (overcharge, over-discharge, short circuit), thermal abuse, etc [20, 21]. Generally,

80 Battery Management System (BMS) and Battery Thermal Management System (BTMS)
81 [22, 23] can monitor and control the real-time safety related parameters (temperature,
82 voltage, current, pressure, etc.) to prevent the batteries from being abused. However,
83 the manufacturing defects (loose connection, separator damage, foreign debris) inside
84 the batteries cannot be monitored or controlled by BMS and BTMS, which may still
85 cause thermal runaway of batteries. Passive inhibition methods are required to limit the
86 TR propagation, and thus avoid catastrophic break down of the whole system.

87 Currently, some experimental and simulation works about safety are based on cell
88 level. Saw et al. have improved the safety performance of single cell by studying the
89 surface roughness and coating thickness of boron nitride added on battery casing [24].
90 Coman et al. [25] have studied different processes of cylindrical cell during TR in a
91 model with venting and quantified the mass fraction of electrolyte leaving the cell can.
92 In addition, there are a few researches aiming at enhancing the safety of battery module.
93 Guo et al. [26] have developed three-dimensional thermal abuse model on the high
94 capacity lithium-ion batteries, which contributes to the design of cooling system in the
95 battery packs. In the normal working status, a 3D thermal model of lithium-ion battery
96 pack is developed to simulate the thermal behaviors of the EV power battery [27].
97 What's more, there are some novel thermal studies about battery module: aluminum
98 foam with porosity control used as cooling system [28], influence of discharging
99 treatment and module shape on the thermal failure propagation [29], and the impact of
100 electrical connections on 18650 cell TR propagation and failure behaviors of pouch
101 cells [30], etc. Abada et al. [31] summarized the phenomenon, mechanism and safety
102 approach of thermal runaway in both cell level and module level.

103 For different kinds of ESS, a price and weight competitive safety grouping scheme
104 is needed to improve the TR resistance of the lithium battery module. Therefore, we
105 proposed four interstitial materials (air, Al plate, graphite composite sheet and Al
106 extrusion) with different potential application values, and studied their inhibition
107 effects on TR propagation. The system studied in this paper is a simplified form of a
108 certain module in the battery pack, which contains 11 parallel cells with various TR
109 propagation paths once TR occurs, and we call it Basic Safety Unit (BSU). Different

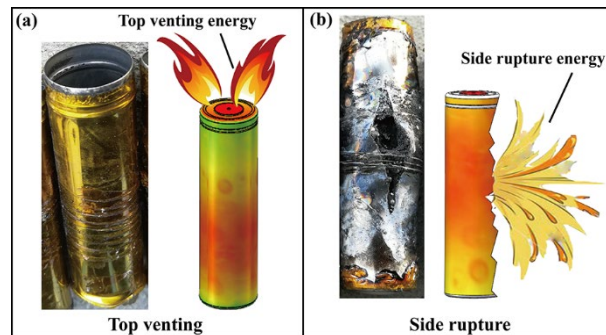
110 interstitial materials are inserted between cells to investigate their effects on thermal
111 inhibition, and the middle cell of the module was heated into TR in the mode of top
112 venting or side rupture. The TR propagation results were studied in both simulation and
113 experimental methods.

114

115 **2. Development of Thermal Model**

116 *2.1 Thermal runaway mechanism*

117 The understanding of the mechanism of TR in a lithium-ion cell is critical when
118 designing the thermal management systems, which should mitigate the effects of TR
119 and impede cell-to-cell propagation. TR means uncontrolled temperature rise of a single
120 cell caused by the exothermic chain reactions and is characterized by a distinct rapid
121 increase of temperature, rather than a steady temperature rise. Energy released during
122 TR in a cell includes cell body energy, top venting energy and side rupture energy, as
123 shown in Fig. 1. The heat released from an abused cell can activate chain reactions in
124 the neighboring cells, causing catastrophic failure of the whole battery module or pack.
125



126

127 **Fig. 1.** Schematic of energy constitution (Physical and model drawing).

128 A TR propagation model was built to analyze the heat transfer through different
129 paths. To simplify the analysis and to focus on the propagation process, some
130 assumptions are proposed as follows [32-34]: the heat transfer condition of TR is set to
131 be adiabatic; residual burning is not considered; the cell is considered as a thermally
132 lumped system; vented gases are not considered as reactive and no combustion is taking
133 place in between the cells. Structural integrity and material properties are assumed to

134 be constant at high temperatures. Every cell conforms to the energy balance equation,
 135 as illustrated in Fig. 2 [35]. The increase of the internal energy of each cell is determined
 136 by the heat generation inside the cell and the heat dissipation rate. The heat generation
 137 is induced by chemical reaction and Joule heating due to electrical short circuit. The
 138 heat dissipation includes conduction, convection and radiation.

$$\begin{array}{c}
 \text{Internal} \\
 \text{Energy change} \\
 \Delta E \\
 \downarrow \\
 mC_p \frac{dT}{dt} \\
 \text{Temp} \\
 \text{rise}
 \end{array}
 =
 \begin{array}{c}
 \text{Heat} \\
 \text{generation} \\
 \dot{Q}_{gen} \\
 \downarrow \\
 \dot{Q}_r + \dot{Q}_s \\
 \text{Chemical} \quad \text{Electrical} \\
 \text{reaction} \quad \text{short}
 \end{array}
 +
 \begin{array}{c}
 \text{Heat} \\
 \text{dissipation} \\
 \dot{Q}_{ht} \\
 \downarrow \\
 \nabla(\lambda \nabla T) - hA(T - T_f) - \varepsilon \sigma A(T^4 - T_w^4) \\
 \text{Heat} \quad \text{Heat} \quad \text{Heat} \\
 \text{conduction} \quad \text{convection} \quad \text{radiation}
 \end{array}$$

139

140

Fig. 2. Energy balance equation of a single cell.

141 In the normal working conditions, \dot{Q}_s is the main source of the heat generation.
 142 When TR occurs in the system, the energy release rate due to chemical reaction \dot{Q}_r
 143 is much larger than \dot{Q}_s from Joule heating rate [32], thus only the effect of \dot{Q}_r is taken
 144 into consideration. Generally, \dot{Q}_r contains the following four parts:

$$145 \quad \dot{Q}_r = \dot{Q}_f + \dot{Q}_n + \dot{Q}_p + \dot{Q}_e \quad (1)$$

146 Where \dot{Q}_f is the heat generation rate due to the decomposition of SEI, \dot{Q}_n due to
 147 Negative-Solvent reaction, \dot{Q}_p due to Positive-Solvent reaction, and \dot{Q}_e is the heat
 148 generation rate due to the decomposition of electrolyte.

149 The heat dissipates from the system to the surroundings through convection and
 150 radiation, and can be written as follows:

$$151 \quad \dot{Q}_{conv} = h_{conv}A(T - T_f) \quad (2)$$

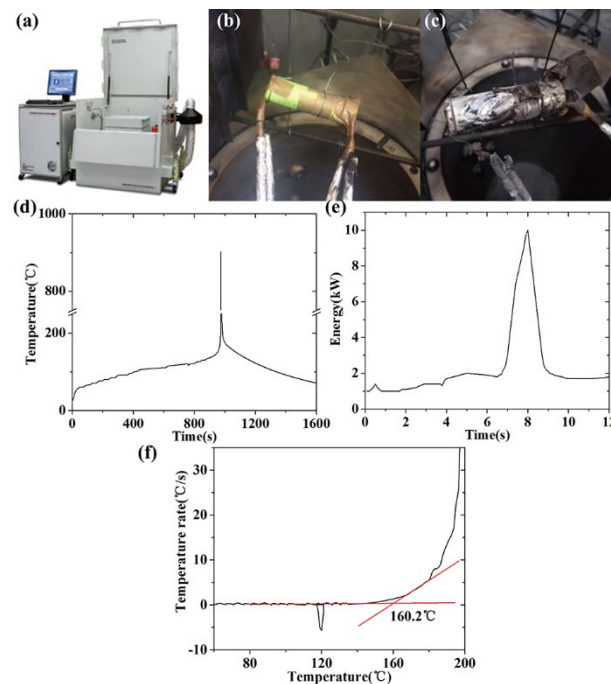
$$152 \quad \dot{Q}_{rad} = \varepsilon \sigma A(T^4 - T_w^4) \quad (3)$$

153 Based on energy balance equations as shown in Eq. (1) - (3), the temperature
 154 distribution inside the system under a certain TR condition can be solved using
 155 numerical simulation tool - FLUENT. The results from the simulation can be used to
 156 predict the most possible location where TR occur and make it possible to prevent it
 157 from happening in advance.

158 2.2 Calibration of thermal properties of single cells

159 Accelerating rate calorimeter (EV-ARC, Thermal hazard technology, UK) was
160 used to measure the thermal hazard and runaway characteristics of commercial 18650
161 lithium-ion batteries, as shown in Fig. 3(a). The thermal runaway energy distribution
162 can be calibrated during the experiment [32, 35]. The change of the temperature during
163 TR is recorded in an adiabatic environment, as shown in Fig. 3(b) & (c).

164 A standard heat-wait-search (HWS) procedure is the most characteristic and
165 prevalent way to determine the onset temperature of self-heating. The tests evaluated
166 the thermal hazard characteristics, such as initial exothermic temperature (T_0) and self-
167 heating rate (dT/dt), as shown in Fig. 3 (d) & (e). The maximum self-heating power of
168 commercial 18650 cylindrical lithium-ion battery cells (Samsung 18650-33G) of 100%
169 state of charge (SOC) was measured to be 9.95 kW, and the maximum temperature
170 reached 889 °C.



171

172 **Fig. 3.** Accelerating rate calorimeter (ARC) test process. (a)ARC test device; (b) & (c) Cell status
173 before & after ARC test; (d) Thermal runaway temperature of a cell; (e) energy release variation
174 curve of a cell; (f) Temperature rate as a function of temperature, T_0 was defined as the point at
175 which the heating-rate curve rises from constant to quasi-exponential.

176 After the experiment proceeded for 960 seconds, it was recorded that the rate of

177 the temperature rise of the cell increased rapidly. T_0 was defined as the point at which
 178 the heating-rate curve rises from constant to quasi-exponential [36], and was used as
 179 the TR triggering temperature (TR_T) to determine if the cell was forced into TR in
 180 simulation. T_0 was 160.6 ± 1.2 °C on average recorded from 8 repeated tests. Fig. 3 (d),
 181 (e) & (f) is the ARC test result from one cell. Cell temperature went up to 889 °C within
 182 a few seconds. The heat generation of the cell during TR was estimated with following
 183 equations:

$$184 \quad C_{total} = \frac{(C_{cell}m_{cell} + C_{can}m_{can})}{(m_{cell} + m_{can})} = 1100 \text{ Jg}^{-1}\text{K}^{-1} \quad (4)$$

185 Where C_{total} is the average mass specific heat of single cell, C_{cell} the average mass
 186 specific heat of the vented cell materials, C_{can} the average mass specific heat of the can
 187 and cell material residual, m_{cell} the mass of the cell materials, m_{can} the mass of the
 188 stainless steel can and m_{total} is the total mass of the single cell. According to the
 189 measurements:

$$190 \quad m_{total} = m_{cell} + m_{can} = 0.047 \text{ kg} \quad (5)$$

$$191 \quad Q_{total} = m_{total}C_{total}\Delta T = 0.047 \times 1100 \times (889 - 160.6) = 37658.28 \text{ J} \quad (6)$$

$$192 \quad Q_{can} = m_{can}C_{can}\Delta T = 4374 \text{ J} \quad (7)$$

$$193 \quad Q_{cell} = Q_{total} - Q_{can} = 33284.28 \text{ J} \quad (8)$$

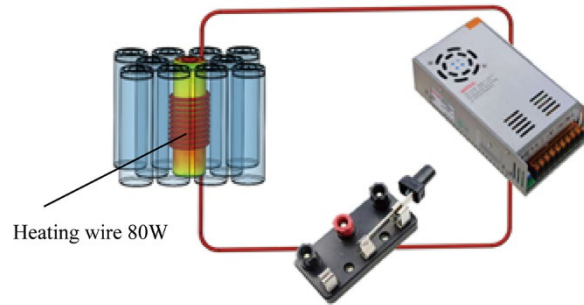
$$194 \quad Q_{cell}/Q_{total} = 33284.28/37658.28 = 0.88 \quad (9)$$

195 Where Q_{total} is the total energy released by the TR cell, Q_{can} is the energy of the can and
 196 cell material residual, and Q_{cell} is the energy carried by the vented cell materials.

197

198 2.3 Experimental study of TR propagation within a test unit

199 There are several methods to initiate the TR such as nail penetration, heating and
 200 overcharge. This study used electrical resistance (Joule) heating to drive the cell into
 201 TR (Fig. 4).



202

203

Fig. 4. Schematic of triggering process of thermal runaway by heating.

204

205

206

207

208

209

210

211

212

213

During the experiment, the triggering cell was heated to TR and forced to release energy in the form of top venting or side rupture. A gas vent is located at the top of the 18650 cell to allow for an internal pressure release when gas builds up inside the cell. Large amount of gas generated inside the cell at TR state would sharply increase internal pressure which could mostly activate the gas vent and release gas from the top of the cell. The practical application of the technique to avoid side rupture is to weaken the strength of the top or the base of cell [37]. Therefore, based on the contrary concept, the top of the cell was enhanced to increase the chance of side rupture. In this experiment, the top of the cell was glued and attached with a metal plate for reinforcement to achieve side rupture intentionally.

214

215

216

217

218

219

220

221

222

223

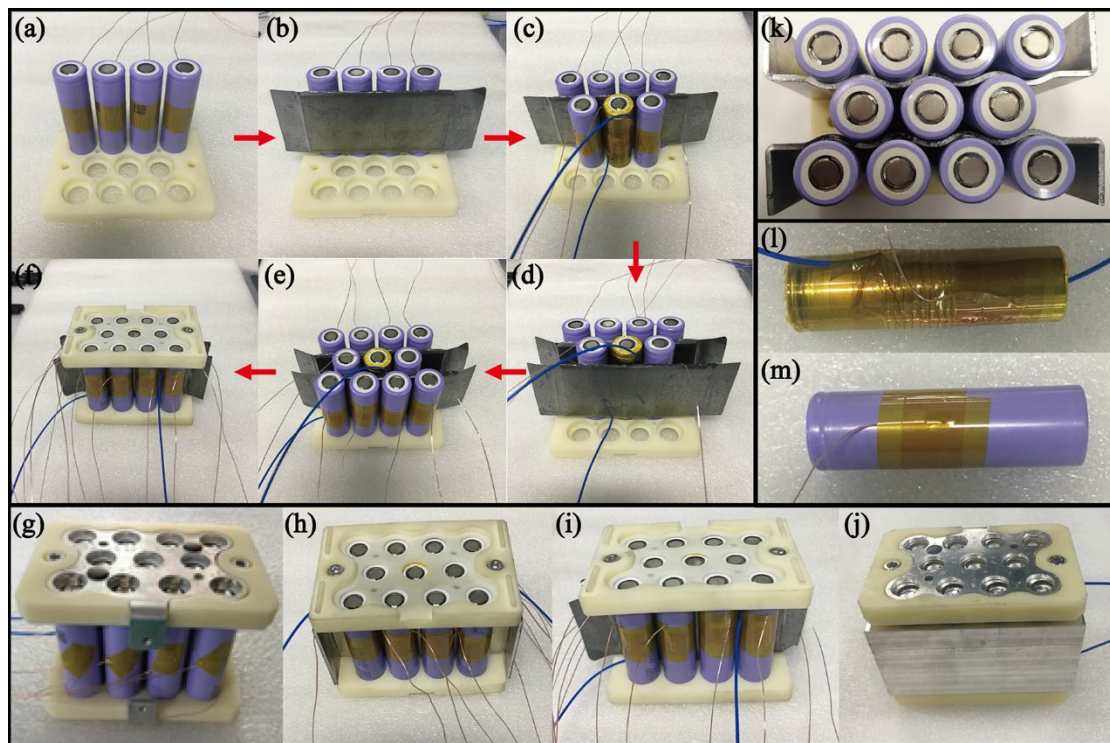
224

225

Commercial cells (Samsung 18650-33G) were used, which are brand new and on-purpose purchased for the experiment. The anode material of the cell is NCA (NiCoAl), the cathode material is graphite, and the electrolyte is mainly ethylene carbonate (EC) with LiPF_6 . Cells were assembled into a BSU and the assembly procedure is illustrated in Fig. 5 (a)-(d). Cells were set between two symmetrical ABS plastic sheet, and the battery spacing were kept 2 mm. A resistance heating wire ($\text{Cr}_{20}\text{Ni}_{80}$) was wound around cell #7 in the central section of the cell (Fig. 5 (l)) for 8 rounds. The winding area accounts for half of the surface area of the cell. Cell #7 was heated during the experiment as triggering cell. The thermal couples were erected against the central surface of each cell, located on the side away from cell #7 (Fig. 5 (e), (m), Fig. 6 (c)). The signals from the thermal couples were collected by a data logger (LR8400-21, HIOKI Japan) (Fig. 7(b)), and the temperatures of the cells were recorded in real time.

226 Different materials were inserted in the interval between the cells, and their materials
 227 are listed in Table 2. The arrangements of interstitial layers are illustrated in Fig. 5(g)-
 228 (j). The thickness of both Al plates and graphite sheets are 2.1 mm. When BSU is
 229 assembled, the cell and the interstitial material are closely contacted (Fig. 5 (k)). BSU
 230 is locked by bolts. Tiny gaps are inevitable but can be ignored in the actual assembly.
 231 It should be noted that the graphite sheets are sandwich structures. And the outer layers
 232 are graphite (0.2 mm thickness) with the thermal conductivity of $800 \text{ W m}^{-1} \text{ K}^{-1}$ in plane
 233 direction and $25 \text{ W m}^{-1} \text{ K}^{-1}$ in axial direction, while the middle layer (1.7 mm thickness)
 234 is a thermal barrier with the thermal conductivity of $0.02 \text{ W m}^{-1} \text{ K}^{-1}$.

235



236

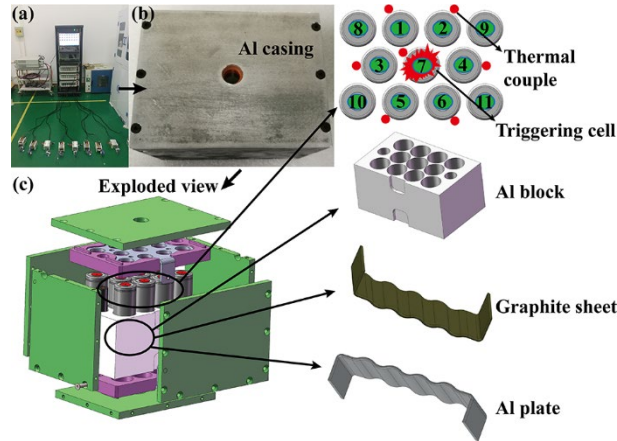
237 **Fig. 5.** Photographs of BSU modules with different interstitial material. (a)-(d) Assembling
 238 procedure for BSU (with graphite sheet); (g)-(j) BSU with different interstitial materials: (g) Air
 239 (natural state), (h) Al plate, (i) Graphite composite sheet, (j) Al extrusion; (k) top view of uncovered
 240 BSU; (l) triggering cell binding with heating wire and thermal couple in the central section of the
 241 cell; (m) neighboring cell binding with a thermal couple.

242

243 Eight BSUs were assembled with 4 interstitial materials and 2 venting options. All
 244 the BSUs were charged to 100% SOC (Fig. 6(a)) and sealed in a casing made of
 aluminum (Fig. 6(b)). The Al casing has a gas vent on the top. Fig. 6 shows an exploded

245 view, which exhibits the configurational structure. The Al casing structure was settled
 246 into a test chamber (1000 mm x 500 mm x 500 mm, 3 mm thickness, made of steel) as
 247 shown in Fig. 7(a) for experiment, which simulated the TR in a battery pack and ensured
 248 safety.

249



250

251 **Fig. 6.** Photograph and schematic of a BSU. (a) Charging setup for BSU. (b) BSU sealed in Al
 252 casing. (c) BSU configuration showing cell numbers and locations of triggered cell (cell 7) and
 253 adjacent cells (cell 1-10). Thermal couples were placed on cell 1-7, while their positions are
 254 represented by red dots.

255



256

257 **Fig. 7.** Devices for thermal runaway experiment

258 During the experiment, the heating wire heated up cell #7 at power of 80 W by the
 259 resistance heating wire until cell #7 run into TR. The temperatures of all cells were
 260 recorded in real time.

261 **Table 2**

262 Characteristics of Samsung 18650-33G and different interstitial materials

Item	Density (kg m ⁻³)	Cp(J kg ⁻¹ K ⁻¹)	Thermal Conductivity(W m ⁻¹ K ⁻¹)
------	----------------------------------	--	--

Samsung 18650-33G	2800	1143	Radial	Axial
			5	1
Al plate	2700	880	230	230
Graphite composite sheet (lightweight)	2200	700	plane/axial	barrier
			800/25	0.02
Al extrusion	2700	880	230	230

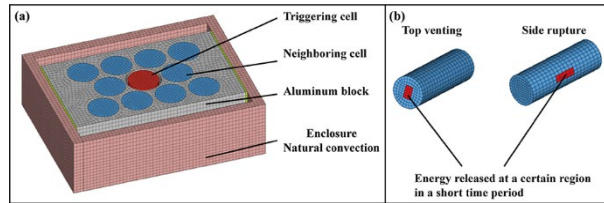
263

264 *2.4 Simulation process*

265 The simulation is based on the BSU containing 11 cells in parallel with various
 266 interstitial materials. The center cell was triggered into energy releasing in the form of
 267 top venting or side rupture. The released energy was transferred to the neighboring cells
 268 through conduction, convection (natural and forced convection) and radiation.
 269 Interstitial materials are directly in contact with the enclosure of BSU, which exchanges
 270 heat with surroundings by convection, as shown in Fig. 6. Mesh of the model is
 271 established by the meshing tool Hypermesh. Nodes between the cell and the interstitial
 272 material and those between the interstitial material and the enclosure are
 273 continuous/uninterrupted, as shown in Fig. 8(a).

274 Finite element method software - Fluent [38] is employed to simulate and analyze
 275 the ability of various interstitial materials to restrain the temperature rise of the
 276 neighboring cells, and furthermore supply theoretical guidance for the TR propagation
 277 in battery module level. The maximum temperature of each single cell will be achieved
 278 during the simulation process. Boundary conditions of the simulation are as follows:
 279 ambient temperature is 27 °C; the Al casing is set to have a gas vent in the top to
 280 simulate the real situation of the cell in a module; the gas ejected during the top venting
 281 is exhausted outside the casing, while the gas ejected during the side rupture is
 282 contained in the casing; the heat exchange between Al casing and external environment
 283 is natural convection with gravity; the battery casing is in intimate contact with the
 284 interstitial material. The middle cell of the module is set to release energy in the form
 285 of top venting and side rupture as shown in Fig. 8(b). Graphite composite sheet and Al

286 plate are in direct contact with the surface of cell body, and the interface contact thermal
287 resistance is ignored. In side rupture condition, hot gas energy is contained within the
288 enclosure.



289
290 **Fig. 8.** Simulation model diagram. (a) Schematic of model mesh for numerical simulation; (b) Two
291 modes of energy releasing: top venting and side rupture.

292 The simulation model is composed of enclosure, ABS plastic plates, thermal pad,
293 four kinds of interstitial materials, cells with 2 mm gap, which is the same as the
294 experiments. For comparison purpose, two mesh sizes (0.5 mm and 1 mm) are
295 produced with 2.33 M and 0.6 M structured meshes, respectively. And nodes are
296 continuous between meshes. No difference is observed between two results. For faster
297 calculation convergence, 1 mm mesh size and continuous nodes between meshes is set
298 for simulation. The ambient temperature is set at 27 °C and material properties are
299 shown in Table 2. The quantified energy released by the triggering cell is illustrated
300 in Fig. 3(d) & (e) and Eqs. (4)-(8). And the heat transfer coefficient of convection
301 between the shell and the ambient surrounding is 5 W m⁻² K⁻¹.

302

303 **3. Results and discussion**

304 The presented work details the TR propagation behavior of the BSUs with both
305 simulation and experiment methods. The center cell was heated into TR. Meanwhile,
306 the temperatures of the center cell and 6 abutting cells were monitored in real-time
307 during the experiments. Experimental and simulation results with different interstitial
308 materials are elaborated in Fig. 9 and Fig. 10, separately.

309 *3.1 Experimental results*

310 Eight BSUs with four different interstitial materials were tested. Cell #7 at the
311 center was heated to TR in the mode of either top venting or side rupture, and the

312 temperatures of cells were recorded. Experimental results are shown in Fig. 10. The
313 relationship between the serial number and the interstitial materials is the same as that
314 in Table 3. Table 3 summarizes the results of each BSU, including TR_T and the time to
315 TR of cell #7, maximum temperature and TR values of neighboring cells.

316 (a) BSU with none interstitial material and top venting mode:

317 TR was triggered in cell #7 after it was heated for 160 s and TR_T was recorded as
318 178 °C approximately. Then the temperature of the adjacent cells rose from 33 °C. The
319 temperatures recorded exceeded the TR temperature (160.6 °C), which means the
320 occurrence of TR propagation. It should be noted that the temperature of adjacent cells
321 around cell #7 fluctuated drastically, which might due to the unstable sporadic,
322 intermittent hot vapor released by the surrounding TR cells.

323 The temperature recorded to reach TR of the experimental module is greater than
324 TR_T of the ARC test on single cell. The reason is that ARC test is a slow heat-wait-
325 search process under the assumption of uniform temperature within the cell. While in
326 the BSU tests, the heating wire heats up the cell from outside at a much higher rate, and
327 the nonuniformity of the temperature within the cell is significant. Therefore, the
328 temperature at the outer shell of the cell is several degrees higher than that at inner part
329 of the cell, which is the criterial to trigger TR. In the following cases, there are also
330 varying degrees of temperature differences.

331 (b) BSU with none interstitial material and side rupture mode:

332 The temperature of cell #7 reached TR_T of 182 °C after it was heated for 115 s.
333 Almost immediately the temperature of the adjacent cells rose sharply and TR
334 propagation occurred. The temperature dropped slowly not until after 350s. The
335 temperature of cell #1 rose much slower than other cells. This may due to the reason
336 that the side rupture direction of cell #7 is facing off the direction of cell #1. Therefore,
337 cell #1 is not directly affected by the explosion, but is subjected to relatively slow heat
338 radiation.

339 (c) BSU with Al plate as interstitial material and top venting mode:

340 The temperature of cell #7 reached TR_T of 184 °C after it was heated for 240 s.
341 There were small fluctuations of the adjacent cells' temperatures. The Al plate acts as

342 a heat sink and absorbs the heat energy of cell #7. The maximum temperature of the
343 adjacent cells reached is about 120 °C, and no TR propagation occurs.

344 (d) BSU with Al plate as interstitial material and side rupture mode:

345 Cell #7 was forced to TR after heated for 240 s. The temperatures of adjacent cells
346 rose sharply along with the TR of cell #7, and TR propagation occurred in the BSU.
347 The energy released by side rupture of cell #7 is all wrapped in the module. The Al
348 plate is saturated as heat sink. Therefore, the heat energy is transferred to the
349 surrounding cells. In the case of top venting (c), part of the energy was released outside
350 the module along with the material explosion, so no TR propagation was observed in
351 Fig. 17(c). The direction of side rupture might face to cell #2, #4, and #6, so the
352 temperature of these cells rose faster than cell #1, #3, and #5 as shown in the inset of
353 Fig. 17(d). Moreover, due to the heat sink and space isolation effect of the aluminum
354 plate, the energy dissipation is relatively stable during the cooling process of the entire
355 module, so the temperature drop is relatively stable compared to (a) and (b).

356 (e) BSU with graphite composite sheets as interstitial material and top venting
357 mode:

358 Cell #7 was heated to trigger TR. Moderate temperature rise (slightly above 100
359 °C) of the adjacent cells was recorded and no TR propagation was observed, as in the
360 case of (c). Furthermore, the maximum temperature of the triggered cell reached about
361 800 °C, and is much smaller than those in modules with TR propagations, which is
362 above 1000 °C. This is due to the large amount of energy released during TR
363 propagations in the modules causing excessive temperature rise in the center of the
364 modules.

365 (f) BSU with graphite composite sheets as interstitial material and side rupture
366 mode:

367 The temperature of the center cell reached TR_T of 178 °C after it was heated for
368 150 s. Moderate temperature rise of the adjacent cell that is directly in the rupture
369 direction of the TR cell was recorded. And no TR propagation was observed after
370 temperature rise fluctuations. Hence, graphite composite sheet can prevent TR
371 propagation in BSU even in the side rupture mode. The graphite sheet has a high

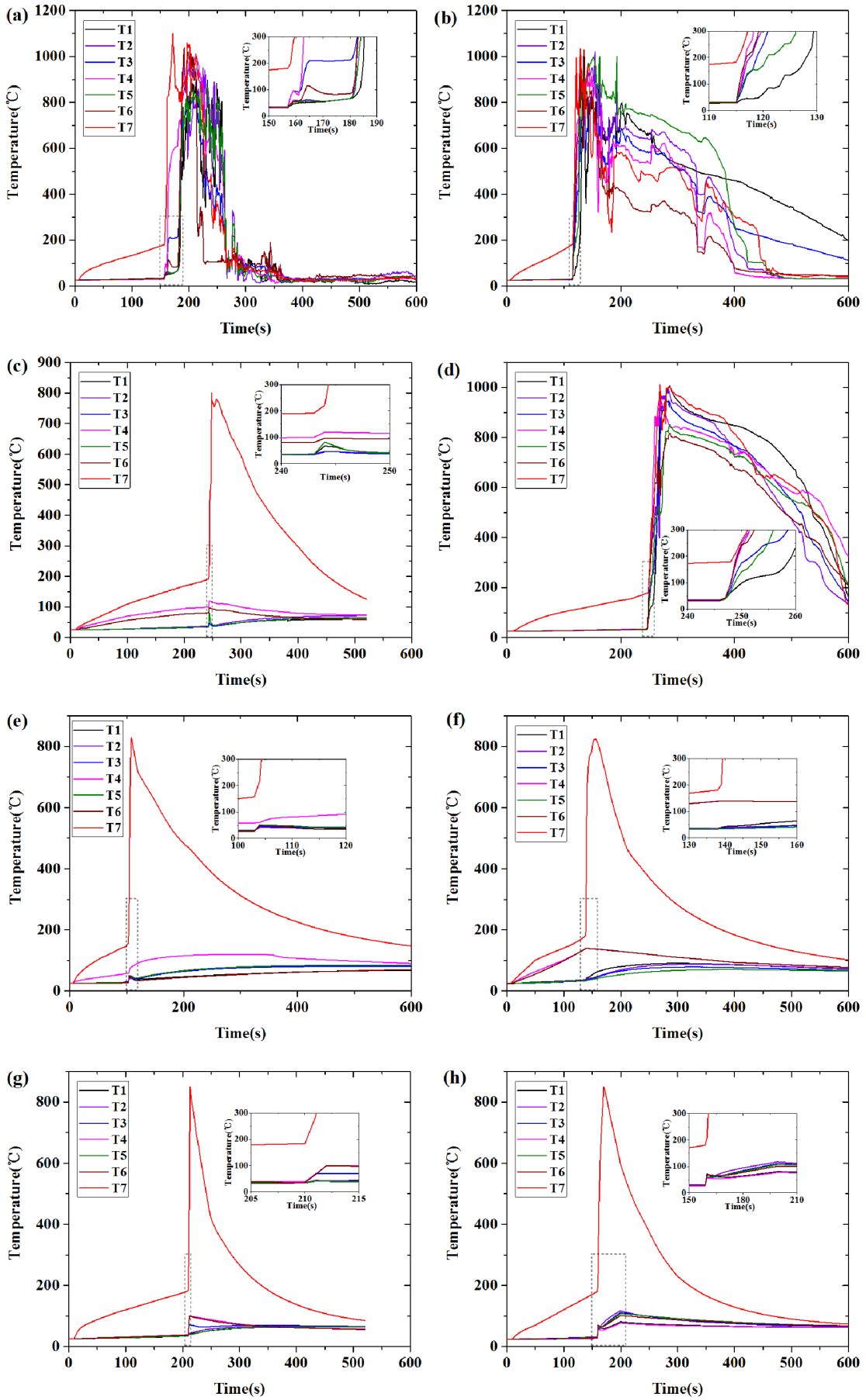
372 thermal conductivity in plane direction ($800 \text{ W m}^{-1}\text{K}^{-1}$), which can spread out the heat
373 released from the TR cell rapidly to the Al casing. On the other hand, the graphite sheet
374 has a low thermal conductivity in the axial direction ($25 \text{ W m}^{-1}\text{K}^{-1}$) due to the sandwich
375 structure, which can effectively shelter the cells adjacent to the TR cell. Therefore, the
376 temperature distribution among the whole module is quite uniform even in this side
377 rupture mode.

378 (g) BSU with Al extrusion as interstitial material and top venting mode:

379 Cell #7 was forced to TR. TR lasted for around 10 s and the maximum temperature
380 reached $850 \text{ }^\circ\text{C}$. The temperature of the neighboring cell 3 reached highest value of 102
381 $^\circ\text{C}$, which did not trigger TR and the rest cells remained stable.

382 (h) BSU with Al extrusion as interstitial material and side rupture mode:

383 Cell #7 was forced to TR. The temperature of adjacent cell #2 reached a maximum
384 temperature around $115 \text{ }^\circ\text{C}$, and did not trigger TR.



386 **Fig. 9.** Experiment results of 7 cells (a) with air as interstitial material and top venting; (b) with air
 387 as interstitial material and side rupture; (c) with Al plate as interstitial material and top venting; (d)
 388 with Al plate as interstitial material and side rupture; (e) with graphite sheet as interstitial material
 389 and top venting; (f) with graphite sheet as interstitial material and side rupture; (g) with Al extrusion
 390 as interstitial material and top venting; (h) with Al extrusion as interstitial material and side rupture.
 391

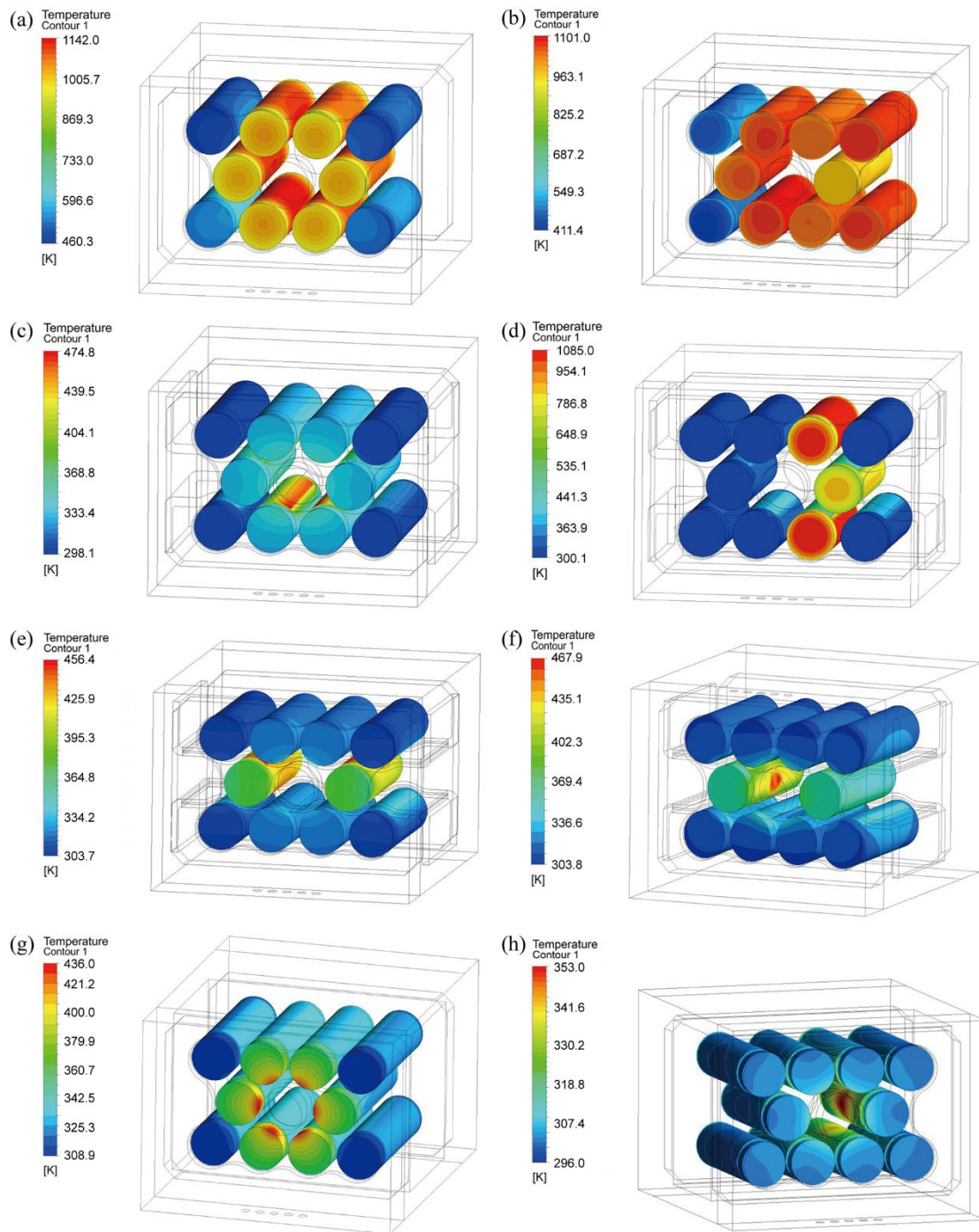
392 **Table 3**

393 Summary of experiment results of all BSUs. The results include venting mode, triggering
 394 temperature and time to TR of cell #7, maximum temperatures and TR values of neighboring cells.
 395 'T' means 'Top venting', 'S' means 'Side rupture'. 'Fail' means that TR propagation occurs in the
 396 module, while 'Pass' means that no TR propagation occurs in the module

	(a)	(b)	(c)	(d)	(e)	(f)	(g)	(h)
Interstitial material	Air(air)		Al plate		graphite composite sheet		Al extrusion	
Venting mode	T	S	T	S	T	S	T	S
Time to TR (s)	160	115	240	240	248	150	210	159
TR _T (°C)	178	182	184	180	157	178	184	181
Max Temp (°C)			120		100	120	102	115
TR value	Fail	Fail	Pass	Fail	Pass	Pass	Pass	Pass

397

398 *3.2 Simulation results*



399

400 **Fig. 10.** Simulation results of the temperature responses of BSU (a) with air as interstitial material
 401 and top venting; (b) with air as interstitial material and side rupture; (c) with Al plate as interstitial
 402 material and top venting; (d) with Al plate as interstitial material and side rupture; (e) with graphite
 403 sheet as interstitial material and top venting; (f) with graphite sheet as interstitial material and side
 404 rupture; (g) with Al extrusion as interstitial material and top venting; (h) with Al extrusion as
 405 interstitial material and side rupture.

406 Fig. 10 illustrates the numerical simulation results of the temperature distribution

407 inside the modules with various interstitial materials. The center cell was hidden to
 408 strengthen the color difference generated from the temperature gradient since the
 409 temperature difference between neighboring cells and the center cell are drastic during
 410 the energy release process. The energy generated by chain reactions is ignored in order
 411 to reduce the complexity of simulation. It is a low cost method to evaluate the safety
 412 and reliability of module design to obtain a simple and clear criterion of thermal
 413 runaway onset. During the simulation, the energy is loaded on the center cell, whose
 414 value is determined from the ARC test. The temperature of the center cell increased to
 415 about 800 °C within 5 s after it was triggered. The neighboring cells reach their peak
 416 temperature after the center cell does. In the experiment process, the thermal couple of
 417 cell #1-#6 was erected against the central surface of each cell, located on the side facing
 418 off from cell #7 (Fig. 6 (c)). In the simulation, the temperatures of neighboring cells are
 419 monitored at locations that are facing away from the center cell, which are the same as
 420 those in the experiment. These recorded temperatures are taken as the criteria of thermal
 421 runaway onset. Sample illustration of simulated temperature results for neighboring
 422 cells is shown in Fig. 11. Temperatures rise rapidly for cells with none interstitial
 423 material and top venting mode (Fig. 11(a)), and no high temperature is found for cells
 424 with Al extrusion and side rupture mode (Fig. 11(b)). The temperatures and outcomes
 425 are shown in Table 4. The triggering temperature is 160.6 ± 1.2 °C acquired from ARC
 426 test.

427

428 **Table 4**

429 Max temperature of neighboring cells in simulation. 'T' means 'Top venting', 'S' means 'Side
 430 rupture'. 'Fail' means that TR propagation occurs in the module, while 'Pass' means that no TR
 431 propagation occurs in the module

No.	(a)	(b)	(c)	(d)	(e)	(f)	(g)	(h)
Interstitial material	None(air)		Al plate		graphite composite sheet		Al extrusion	
Venting mode	T	S	T	S	T	S	T	S
Cell Temp.(°C)	869	828	80	812	153	120	83	80

TR value Fail Fail Pass Fail Pass Pass Pass Pass

432

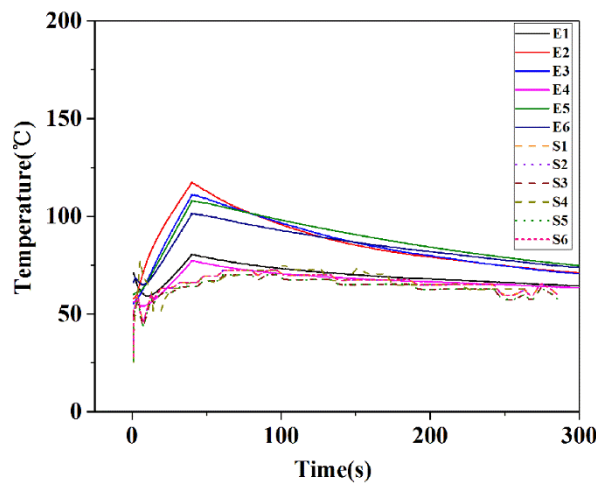
433 *3.3 Summary*

434 **Table 5**

435 Results of TR experiment. 'Pass' means no TR propagation occurring in the BSU, while 'Fail' means
 436 TR propagation occurring in the BSU.

Interstitial material	Mode	Simulation	Experiment
		results	results
Air	Top venting	Fail	Fail
	Side rupture	Fail	Fail
Al plate	Top venting	Pass	Pass
	Side rupture	Fail	Fail
Graphite composite sheet	Top venting	Pass	Pass
	Side rupture	Pass	Pass
Al extrusion	Top venting	Pass	Pass
	Side rupture	Pass	Pass

437



438

439 **Fig. 11.** Temperature results of BSU with Al extrusion as interstitial material and side rupture mode
 440 for both simulation and experiment. Curves “E1-E6” are temperature records of cell #1-#6
 441 in experiment; Curves “S1-S6” are simulation calculated temperature results for cell#1- #6.

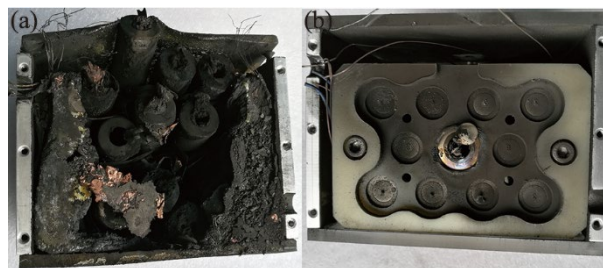
442

Temperature results of BSU with Al extrusion as interstitial material and side

443 rupture mode for both simulation and experiment are shown in Fig. 11. The
444 temperatures of neighboring cells #1-#6 agreed well, which provides a basis for
445 consistency of simulation and experimental results.

446 The simulation and experiment results are summarized in Table 5. The outcomes
447 of the experiments are shown in Fig. 12. Generally, the results of experiment and
448 simulation agreed well, except certain temperature differences. From the simulation and
449 experimental results, it can be seen that under the current module energy density and
450 battery spacing conditions, only air in the gap cannot prevent the TR propagation in any
451 form. In the case of top venting, the aluminum plate has the function of heat sink and
452 heat conductor, which successfully prevents the TR propagation, but is overwhelmed
453 in the case of side rupture. The graphite composite plate and Al extrusion can
454 successfully prevent the TR propagation under both modes (top venting and side
455 rupture). The high in-plane thermal conductivity of the graphite in the graphite
456 composite plate and the thermal insulation of the intermediate interlayer effectively
457 prevent the heat from being transferred to adjacent cells. The Al extrusion can absorb
458 the heat generated from the TR cell as a robust heat sink, which can effectively prevent
459 the TR propagation.

460



461

462 **Fig. 12.** BSUs with (a) and without (b) the propagation of thermal runaway.

463 Graphite composite plates are light in weight but expensive, and are not suitable
464 for common consumer product applications. It is suitable for applications where energy
465 density and safety requirements are relatively high, such as space and military battery
466 unit. The Al extrusion is relatively heavy but has a lower cost than graphite composite
467 sheet, and it can prevent the TR propagation mostly. It can be used in the case of weight-
468 insensitive products such as heavy duty electric machines, energy storage power

469 stations.

470

471 **4. Conclusion**

472 The objective of this study is the inhibition effect on TR propagation utilizing
473 different interstitial materials when TR of a cell occurs in a module. Four interstitial
474 materials were evaluated in both simulation and experimental methods. And the
475 commercial application prospects of the battery module design were also discussed. In
476 this study, modules composed of 11 cells with four interstitial materials (air, Al plate,
477 graphite composite sheet and Al extrusion) were built as the basic test units. The TR
478 conditions and properties of a single cell were calibrated by ARC test. In simulation
479 these properties were loaded on the center cell as initial condition to calculate the
480 temperature distribution of the neighboring cells, while the chain reactions were not
481 considered. The center cell was triggered into TR by an 80W heating wire and the
482 temperature of all the cells were monitored in the experiment process.

483 TR is a drastic energy releasing process, especially in side rupture condition. In
484 battery module design, air alone cannot prevent the TR propagation. Aluminum plate
485 has a certain safety protection against TR, but failed in the case of side rupture. The
486 graphite composite sheet can significantly prevent the TR propagation, due to the high
487 in-plane thermal conductivity of the graphite sheet layers and relatively low thermal
488 conductivity in cross-plane direction of the graphite sheet layers, particularly the high
489 thermal insulation and fire resistance of intermediate layer. Even though Al extrusion
490 is slightly heavy, but it shows the best performance in restraining TR propagation,
491 which can stabilize the temperature of the entire module in a moderate range. This
492 approach is most likely to be applicable for lithium-ion batteries which have an energy
493 density not higher than that used. At present, the results of this study are more inclined
494 to be applied to cylindrical batteries. It may also be useful for prismatic and pouch cells
495 with higher energy, while the structure design and material parameters need to be
496 further adjusted according to different application states.

497 It can be seen that side rupture of the triggering cell can significantly increase the

498 possibility of TR propagation and managing the top venting path is critical for thermal
499 management. It is a feasible way to improve the safety of the high specific energy
500 lithium ion battery by utilizing different interstitial materials to change the thermal path
501 in the battery module. A proper safety valve should be designed in the bottom of cell to
502 release the pressure and heat, which is a critical means to help avoiding side rupture.
503 Furthermore, for safety concern, the combustion of expelled electrolyte must be
504 directed away from adjacent cells in the battery packs.

505

506 **Acknowledgments**

507 This work was supported by the National Natural Science Foundation of China
508 (#11572311 and #11772321) and the Chinese 1000 Young Talented Program. The
509 authors wish to thank USTC Center of Micro and Nanoscale Research and Fabrication
510 for providing the experimental facilities used in this work.

511

512 **References**

- 513 [1] X. Shan, F. Li, D. Wang, H. Cheng, The smart era of electrochemical energy storage devices,
514 Energy Storage Mater. 3 (2016) 66-68.
- 515 [2] J.B. Dunn, L. Gaines, J.C. Kelly, C. James, K.G. Gallagher, The significance of Li ion batteries
516 in electric vehicle life-cycle energy and emissions and recycling's role in its reduction, Energy
517 Environ. Sci. 8 (2015) 158-168.
- 518 [3] D. Liu, H. Wang, Y. Peng, W. Xie, H. Liao, Satellite lithium-ion battery remaining cycle life
519 prediction with novel indirect health indicator extraction, Energies 6 (2013) 3654-3668.
- 520 [4] E. Darcy, Thermal runaway Severity Reduction Assessment for EVA Li-ion Batteries,
521 Huntsville, Alabama, 2014.
- 522 [5] W. Walker, S. Yayathi, J. Shaw, H. Ardebili, Thermo-electrochemical evaluation of lithium-
523 ion batteries for space applications, J. Power Sources 298 (2015) 217-227.
- 524 [6] Y. Xie, J. Tang, S. Shi, Y. Xing, H. Wu, Z. Hu, Experimental and numerical investigation on
525 integrated thermal management for lithium-ion battery pack with composite phase change

526 materials, *Energy Convers. Manage.* 154 (2017) 562-575.

527 [7] C. Lopez, J. Jeevarajan, P. Mukherjee, Experimental analysis of thermal runaway and
528 propagation in lithium-ion battery modules, *J. Electrochem. Soc.* 162 (2015) 1905-1915.

529 [8] A.W. Golubkov, D. Fuchs, J. Wagner, H. Wiltsche, C. Stangl, G. Fauler, et al., Thermal-
530 runaway experiments on consumer Li-ion batteries with metal-oxide and olivin-type cathodes,
531 *RSC Adv.* 4 (2014) 3633-3642.

532 [9] X. Feng, X. He, M. Ouyang, L. Lu, P. Wu, C. Kulp, et al., Thermal runaway propagation model
533 for designing a safer battery pack with 25Ah LiNix-CoyMnzO2 large format lithium ion
534 battery, *Appl. Energy* 154 (2015) 74-91.

535 [10] W. Wu, X. Yang, G. Zhang, K. Chen, S. Wang, Experimental investigation on the thermal
536 performance of heat pipe-assisted phase change material based battery thermal management
537 system, *Energy Convers. Manage.* 138 (2017) 486-492.

538 [11] A. Melcher, C. Ziebert, M. Rohde, B. Lei, H.J. Seifert, Modeling and Simulation of the
539 Thermal Runaway Behavior of Cylindrical Li-Ion Cells - Computing of Critical Parameters,
540 *Energies* 9 (2016) 292.

541 [12] D.P. Abraham, E.P. Roth, R. Kostecky, K. McCarthy, S. MacLaren, D.H. Doughty, Diagnostic
542 examination of thermally abused high-power Lithium-ion cells, *J. Power Sources* 161 (2006)
543 648-657.

544 [13] D. Hyup Jeon, S. Man Baek, Thermal modeling of cylindrical lithium ion battery during
545 discharge cycle, *Energy Convers. Manage.* 52 (2011) 2973-2981.

546 [14] A. Mills, M. Farid, J.R. Selman, S. Al-Hallaj, Thermal conductivity enhancement of phase
547 change materials using a graphite matrix, *Appl. Therm. Eng.* 26 (2006) 1652-1661.

548 [15] Q. Wang, P. Ping, X. Zhao, G. Chu, J. Sun, C. Chen, Thermal runaway caused fire and
549 explosion of lithium ion battery, *J. Power Sources* 208 (2012) 210-224.

550 [16] R. Walters, R.E. Lyon, Energy release from lithium ion batteries in the bomb calorimeter, in:
551 *Proceedings of the Fire and Materials Conference, San Fran-cisco, 2015* 78-86.

552 [17] X. Xu, R. He, Review on the heat dissipation performance of battery pack with different
553 structures and operation conditions, *Renew. Sustain. Energy Rev.* 29 (2014) 301-315.

554 [18] Z. Rao, S. Wang, A review of power battery thermal energy management, *Renew. Sustain.*
555 *Energy Rev.* 15 (2011) 4554-4571.

- 556 [19] J. Xun, R. Liu, K. Jiao, Numerical and analytical modeling of lithium ion battery thermal
557 behaviors with different cooling designs, *J. Power Sources* 233 (2013) 47-61.
- 558 [20] J. Wen, Y. Yu, C. Chen, A review on lithium-ion batteries safety issues: existing problems and
559 possible solutions, *Mater. Express* 2 (2012) 197-212.
- 560 [21] X. Feng, M. Ouyang, X. Liu, L. Lu, Y. Xia, X. He, Thermal runaway mechanism of lithium
561 ion battery for electric vehicles: A review, *Energy Storage Mater.* 10 (2018) 246-267.
- 562 [22] H. Fathabadi, High thermal performance lithium-ion battery pack including hybrid active-
563 passive thermal management system for using in hybrid/electric vehicles, *Energy*, 70 (2014)
564 529-538.
- 565 [23] J. Zhao, Z. Rao, Y. Huo, X. Liu, Y. Li, Thermal management of cylindrical power battery
566 module for extending the life of new energy electric vehicles, *Appl. Therm. Eng.* 85 (2015)
567 33-43.
- 568 [24] L. H. Saw, Y. Ye, A. A. O. Tay, Feasibility study of Boron Nitride coating on Lithium-ion
569 battery casing, *Appl. Therm. Eng.* 73 (2014) 154-161.
- 570 [25] P. T. Coman, S. Rayman, R. E. White, A lumped model of venting during thermal runaway in
571 a cylindrical Lithium Cobalt Oxide lithium-ion cell, *J. Power Sources* 307 (2016) 56-62.
- 572 [26] G. Guo, B. Long, B. Cheng, S. Zhou, P. Xu, B. Cao, Three-dimensional thermal finite element
573 modeling of lithium-ion battery in thermal abuse application, *J. Power Sources* 195 (2010)
574 2393-2398.
- 575 [27] B. Liu, Three dimensional thermal modeling of lithium-ion battery pack for electric vehicles
576 thermal management, M.Sc. thesis, Hong Kong University of Science and Technology, 2014.
- 577 [28] L. H. Saw, Y. Ye, M. C. Yew, W. T. Chong, M. K. Yew, T. C. Ng, Computational fluid
578 dynamics simulation on open cell aluminium foams for Li-ion battery cooling system, *Appl.*
579 *Energy* 204 (2017) 1489-1499.
- 580 [29] D. Ouyang, J. Liu, M Chen, J Weng and J. Wang, Thermal Failure Propagation in Lithium-Ion
581 Battery Modules with Various Shapes, *Appl. Sci.* 8 (2018) 1263.
- 582 [30] J. Lamb, C. J. Orendorff, L. A. M. Steele, S. W. Spangler, Failure propagation in multi-cell
583 lithium ion batteries, *J. Power Sources* 283 (2015) 517-523.
- 584 [31] S. Abada, G. Marlair, A. Lecocq, M. Petit, V. Sauvart-Moynot, F. Huet, Safety focused
585 modeling of lithium-ion batteries: A review, *J. Power Sources* 306 (2016) 178-192.

- 586 [32] W. Chen, Y. Wang, C. Shu, Adiabatic calorimetry test of the reaction kinetics and self-heating
587 model for 18650 Li-ion cells in various states of charge, *J. Power Sources* 318 (2016) 200-209.
- 588 [33] T. D. Hatchard, D. D. MacNeil, A. Basuc and J. R. Dahn, Thermal Model of Cylindrical and
589 Prismatic Lithium-Ion Cells, *J. Electrochem. Soc.* 148 (2001) 755.
- 590 [34] G. Kim, A. Pesaran, R. Spotnitz, A three-dimensional thermal abuse model for lithium-ion
591 cells, *J. Power Sources* 170 (2007), 476.
- 592 [35] P. Wu, J. Romberg, X. Feng, M. Zhang, L. Lu, X. He, M. Ouyang, Thermal Runaway
593 Propagation Within Module Consists of Large Format Li-Ion Cells. *Proceedings of SAE-China*
594 *Congress 2015: Electrical Engineering* 364.
- 595 [36] A. W. Golubkov, D. Fuchs, J. Wagner, H. Wiltsche, C. Stangl, G. Fauler, G. Voitc, A. Thaler,
596 V. Hacker. Thermal-runaway experiments on consumer Li-ion batteries with metal-oxide and
597 olivin-type cathodes. *RSC Advances* 4(2014) 3633.
- 598 [37] D. P. Finegan, Identifying the Cause of Rupture of Li - Ion Batteries during Thermal Runaway,
599 *Adv. Sci.* 5 (2018) 170-369.
- 600 [38] *Fluent User's Guide: Version 14.0, 2014.*